Frontal Photopolymerization for Microfluidic Applications

João T. Cabral,* Steven D. Hudson, Christopher Harrison, and Jack F. Douglas*

Polymers Division, National Institute of Standards and Technology, Gaithersburg, Maryland 20899

Received February 25, 2004. In Final Form: May 6, 2004

Frontal photopolymerization (FPP) offers numerous advantages for the rapid prototyping of microfluidic devices. Quantitative utilization of this method, however, requires a control of the vertical dimensions of the patterned resist material. To address this fundamental problem, we study the ultraviolet (UV) photopolymerization of a series of multifunctional thiolene resists through a combination of experiments and analytical modeling of the polymerization fronts. We describe this nonlinear spatio-temporal growth process in terms of a "minimal" model involving an order parameter $\phi(x, t)$ characterizing the extent of monomer-to-polymer conversion, the optical attenuation $T(x, t)$, and the solid front position $h(t)$. The latter exhibits an induction time (or equivalent critical UV dose) characterizing the onset of frontal propagation. We also observe a novel transition between two logarithmic rates of growth, determined by the Beer−Lambert attenuation constants μ_0 and μ_∞ of the monomer and fully polymerized material, respectively. The measured frontal kinetics and optical transmission of the thiolene resist materials are consistent with our photopolymerization model, exhibiting both "photodarkening" and "photoinvariant" polymerization. This is apparently the first observation of photodarkening reported in FPP. On the basis of these results, multilevel fluidic devices with controlled height are readily fabricated with modulated illumination. A representative two-level microfluidic device, incorporating a chaotic mixer, a T junction, and a series of controlled flow constrictions, illustrates the practical versatility of this fabrication method.

Introduction

Microfluidics drives an incessant demand for rapid prototyping (RP) techniques[1] capable of fabricating fluid handling devices with increasing complexity, shorter fabrication times, and lower cost. In addition, the broadening of microfluidic applications into materials science requires device chemical compatibility. Indeed, much of the work to date has been restricted to the use of poly(dimethylsiloxane) (PDMS) technology[2−5] and aqueous solutions,[6] while many analytic studies require the use of organic solvents. Photopolymerization of multifunctional monomer resists[7−11] through an optical mask constitutes a simple but powerful lithographic route to RP. Photocuring can be extremely fast, and substantial chemical resistance is achievable with these highly cross-linked networks. Toward this end, we have recently reported a simple RP technique capable of fabricating transparent organic solvent−resistant devices with features of great depth.[12] Our RP method (Figure 1) is based on the contact lithography of an ultraviolet (UV) cross-linkable multifunctional thiolene prepolymer (used as a negative photoresist) and consists of a few simple steps: mask design, resist deposition between transparent substrates, an UV pre-cure through a mask, pattern development, and a flood UV post-cure. The overall process is completed within a few hours, allowing for multiple design iterations during the period of a day. In the present work, we explore the potential of frontal photopolymerization (FPP) for microfluidic device fabrication with increased complexity and enhanced dimensional control.

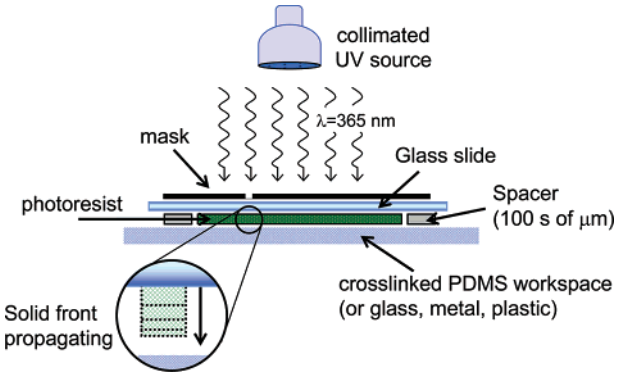

Figure 1. Schematic of the experimental setup showing the collimated 365-nm UV source, photomask, resist material, top and bottom confining surfaces (usually glass/glass or glass/PDMS, respectively), and spacers. The inset depicts a photopolymerization front emanating from the illuminated surface.

Photopolymerization is a complex, nonlinear spatio-temporal process that results in nonuniform monomer-to-polymer conversion profiles orthogonal to the illuminated surface.[7−9] However, these conversion profiles may sharpen into stable planar polymerization *fronts* that move

* Corresponding authors. E-mail: joao.cabral@nist.gov (J.T.C.); jack.douglas@nist.gov (J.F.D.).

(1) Recent reviews on microfluidics and its applications: Whitesides, G. M.; Stroock, A. D. *Phys. Today* **2001**, *54*, 42. Mitchell, P. *Nat. Biotechnol.* **2001**, *19*, 717. Hong, J. W.; Quake, S. R. *Nat. Biotechnol.* **2003**, *21*, 1179. Ismagilov, R. F. *Angew. Chem., Int. Ed.* **2003**, *42*, 4130. Ouellette, J. *Ind. Phys.* **2003**, Aug/Sep, 14.

(2) Duffy, D. C.; McDonald, J. C.; Schueller, O. J. A.; Whitesides, G. M. *Anal. Chem.* **1998**, *70*, 4974.

(3) McDonald, J. C.; Duffy, D. C.; Anderson, J. R.; Chiu, D. T.; Wu, H.; Schueller, O. J. A.; Whitesides, G. M. *Electrophoresis* **2000**, *21*, 27.

(4) Becker, H.; Locascio, L. *Talanta* **2002**, *56*, 267.

(5) McDonald, J. C.; Whitesides, G. M. *Acc. Chem. Res.* **2002**, *35*, 491.

(6) Lee, J. N.; Park, C.; Whitesides, G. M. *Anal. Chem.* **2003**, *75*, 6544.

(7) Odian, G. *Principles of Polymerization*; John Wiley & Sons: New York, 1991.

(8) Fouassier, J.-P. *Photoinitiation, Photopolymerization, and Photocuring*; Hanser/Gardner Publications: Cincinnati, OH, 1995.

(9) *Radiation Curing in Polymer Science and Technology*; Fouassier, J.-P., Rabek, J. F., Eds.; Elsevier Applied Science: London, 1993.

(10) (a) Decker, C. *Polym. Int.* **1998**, *45*, 133; (b) **2002**, *51*, 1141 (reviews photopolymerization and its applications).

(11) Reichmanis, E.; Thompson, L. F. *Chem. Rev.* **1989**, *89*, 1273 (a review of lithography of polymer materials).

(12) Harrison, C.; Cabral, J. T.; Stafford, C.; Karim, A.; Amis, E. J. *J. Micromech. Microeng.* **2004**, *14*, 153.

10.1021/la049501e CCC: $27.50
Published on Web 07/09/2004

as *traveling waves*, in the presence of strong optical attenuation and limited mass and heat transfer. This frontal aspect of the polymerization process is particularly apparent in the photopolymerization (and cross-linking) of thick material sections and has counterparts in degradation (including discoloration) processes in polymer films exposed to UV radiation.[10,13] FPP is a versatile method of polymer synthesis that is utilized in numerous applications, including dental and prosthetic materials, adhesives, and coatings, to name a few.[10]

It should be appreciated that FPP is quite distinct from thermal and isothermal frontal polymerization (IFP) processes, which are essentially autocatalytic in nature and propagate with a constant wave velocity.[14] Front propagation in thermal frontal polymerization is sustained by the thermal energy released from exothermic polymerization. The reaction is initiated by a localized heat source, and rate of front propagation is governed by an interplay of thermal diffusion and the nonlinear temperature dependence of the polymerization rate constants. In IFP, also known as "interfacial gel polymerization", polymerization occurs in a viscous or gel matrix which inhibits chain termination. A self-sustaining polymerization front is initiated by introducing a polymer seed. The history, nature, and applications of these polymerization methods are reviewed by Pojman and co-workers.[15]

Our own interest in FPP stems from its photolithographic potential in RP of microfluidic devices. This capability has already been recognized in stereolithography, a layer-by-layer fabrication technique of three-dimensional polymeric (and ceramic) objects.[16−18] We believe that FPP provides a means to (i) accurately control vertical patterned dimensions by light exposure (independent of resist thickness) and (ii) generate nonplanar, either height-gradient or multilevel, structures for microfluidic devices. The latter is particularly valuable, for example, in the fabrication of passive mixers,[19−21] which are central components in microfluidic devices. Conventionally, multilevel structures are fabricated with rather complex and time-consuming methods such as anisotropic plasma etching,[19] laser ablation,[20] solid-object printing[22] and stereolithography,[16−18] and multilayer photolithography[23] (requiring several photoresist deposition and alignment steps prior to development). Photolithography based on frontal polymerization, on the other hand, can generate multilevel patterns with rapidity and simplicity. Light exposure can be modulated either by a sequence of imaging steps through binary masks or by using gray-scale masks.[24−26]

An effective application of FPP to RP requires a fundamental understanding of its mechanism and growth kinetics. A number of photoinitiation and polymerization models have been recently reported in the literature, notably by Terrones and Pearlstein,[27] Ivanov and Decker,[28] Miller et al.,[29] and Bowman and co-workers.[30] These extensive treatments account for photochemical reaction details having various degrees of complexity, including initiator photolysis, chain initiation, propagation and termination (possible oxygen inhibition), and the resulting chain length distribution.[27c] Particular emphasis is given to following the evolution of photoinitiator concentration in the special case of photobleaching radical polymerizations. A few treatments include additional diffusion mechanisms (of monomer[30b,c] or initiator)[27d,29] and selected mass and or heat transfer processes,[30b,31] concurrent with photopolymerization. The utilization of such models requires the determination of numerous parameters describing the kinetic coefficients and transport properties and their coupling as these variables are changed. This is true even for idealized single-step reactions with first-order kinetics. Given the complexity of these systems, we seek to develop a "minimal" FPP model based on physical observables relevant to RP. In particular, we are concerned with two basic FPP characteristics and their evolution in time: (1) the position of the solid/liquid front, which defines the patterned height, and (2) the light transmission of the resist layer. Our model involves a system of coupled integro-differential equations describing the extent of monomer-to-polymer conversion, $\phi(x, t)$, and the light attenuation $T(x, t)$ as a function of the distance from the illuminating surface x and time t. Despite the simplicity of this model, we find that we can quantitatively describe the evolution of the front position, thus, obtaining a description suitable for the purpose of device fabrication.

We have experimentally studied the photopolymerization kinetics of multifunctional thiolene-based resists. Our choice was motivated by their suitability for microfluidic device fabrication:[12] the pre-polymer (a solvent-free, low-viscosity liquid) photocures into a hard solid, which is optically transparent and impervious to a range of organic solvents. In addition, the resists can attain large cure depths (>1000 μm) and exhibit low shrinkage and good adhesion to glass (and metal) surfaces. Thus, they provide a convenient matrix for fluid handling devices for research in materials science. This is also a favorable system because thiolene based "optical adhesives" are widely

(13) Rytov, B. L.; Ivanov, V. B.; Ivanov, V. V.; Anisimov, V. M. *Polymer* **1996**, *37*, 5695.

(14) A number of phenomena may affect these frontal polymerization processes. Mode coupling (between composition, temperature, and other relevant variables) can lead to periodic oscillations of the propagation velocity. The stability and form of the polymerization front is also influenced by hydrodynamic instabilities and heterogeneities, including bubbles (due to boiling monomer or initiator byproducts), impurities, and boundaries.

(15) (a) Khan, A. M.; Pojman, J. A. *Trends Polym. Sci.* **1996**, *4*, 253. (b) Pojman, J. A.; Ilyashenko, V. M.; Khan, A. M. *J. Chem. Soc., Faraday Trans.* **1996**, *92*, 2825. (c) Lewis, L. L.; DeBisschop, C. A.; Pojman, J. A.; Volpert, V. A. In *Nonlinear Dynamics In Polymeric Systems*; Pojman, J. A., Tran-Cong-Miyata, Q., Eds.; *ACS Symposium Series*; American Chemical Society: Washington, DC, 2004; Vol. 869, p 169.

(16) Flach, L.; Chartoff, R. P. *Polym. Eng. Sci.* **1995**, *35*, 483; **1995**, *35*, 493.

(17) Bertsch, A.; Jézéquel, J. Y.; André, J. C. *J. Photochem. Photobiol., A* **1997**, *107*, 275.

(18) Lee, J. H.; Prud'homme, R. K.; Askay, I. A. *J. Mater. Res.* **2001**, *16*, 3636.

(19) Liu, R. H.; Stremler, M. A.; Sharp, K. V.; Olsen, M. G.; Santiago, J. G.; Adrian, R. J.; Aref, H.; Beebe, D. J. *J. Microelectromech. Syst.* **2000**, *9*, 190.

(20) Johnson, T. J.; Ross, D.; Locascio, L. E. *Anal. Chem.* **2002**, *74*, 45.

(21) (a) Stroock, A. D.; Dertinger, S. K. W.; Ajdari, A.; Mezic, I.; Stone, H. A.; Whitesides, G. M. *Science* **2002**, *295*, 647. (b) Stroock, A. D.; Dertinger, S. K.; Whitesides, G. M.; Ajdari, A. *Anal. Chem.* **2002**, *74*, 5306. (c) Stroock, A. D.; Whitesides, G. M. *Acc. Chem. Res.* **2003**, *36*, 597.

(22) McDonald, J. C.; Chabinyc, M. L.; Metallo, S. J.; Anderson, J. R.; Stroock, A. D.; Whitesides, G. M. *Anal. Chem.* **2002**, *74*, 1537.

(23) Anderson, J. R.; Chiu, D. T.; Jackman, R. J.; Cherniavskaya, O.; McDonald, J. C.; Wu, H.; Whitesides, S. H.; Whitesides, G. M. *Anal. Chem.* **2000**, *72*, 3158.

(24) Kley, E.-B. *Microelectron. Eng.* **1997**, *34*, 261.

(25) Wu, H.; Odom, T. W.; Whitesides, G. M. *Anal. Chem.* **2002**, *74*, 3267.

(26) Chen, C.; Hirdes, D.; Folch, A. *Proc. Natl. Acad. Sci. U.S.A.* **2003**, *100*, 1499.

(27) (a) Terrones, G.; Pearlstein, A. J. *Macromolecules* **2001**, *34*, 8894; (b) **2001**, *34*, 3195; (c) **2003**, *36*, 6346; (d) **2004** *37*, 1565.

(28) Ivanov, V. V.; Decker, C. *Polym. Int.* **2001**, *50*, 113−118.

(29) Miller, G. A.; Gou, L.; Narayanan, V.; Scranton, A. B. *J. Polym. Sci., Part A: Polym. Chem.* **2002**, *40*, 793.

(30) (a) Goodner, M. D.; Bowman, C. N. *Macromolecules* **1999**, *32*, 6552; (b) *Chem. Eng. Sci.* **2002**, *57*, 887. (c) O'Brien, A.; Bowman, C. N. *Macromolecules* **2003**, *36*, 7777.

(31) Belk, M.; Kostarev, K. G.; Volpert, V.; Yudina, T. M. *J. Phys. Chem. B* **2003**, *107*, 10292.

available because of their many commercial applications. Thiolene (i.e., monomers containing mercapto and vinyl groups) polymerization chemistry is relatively well understood,[10b,32,33] and its photopolymerization has recently been examined in detail by Cramer et al.[33] and by Wilderbeek et al. (using liquid crystalline monomers).[34] Autocatalytic frontal polymerization of thiolene systems has been recently demonstrated by Pojman et al.[35] Thiolenes polymerize via a free-radical step growth mechanism (even in the absence of photoinitiator),[33a] exhibiting little oxygen inhibition. The latter (unlike in other radical polymerization mechanisms) is rather advantageous for RP because it allows fabrication in an unprotected atmosphere.[10]

This paper is organized as follows: We first describe an experimental investigation of the propagation of conversion fronts in multifunctional thiolene-based formulations. Both light transmission and front position are measured as a function of exposure UV dose. We then introduce a simple FPP model that accounts for both the "photobleaching" and "photodarkening" effects observed in our measurements. The modeling directly addresses the measurable properties under our control and relevant to RP. We finally describe the fabrication of a microfluidic device on the basis of our FPP methodology.

Experimental Section

Materials.[36] A series of multifunctional thiolene-based optical adhesives were purchased from Norland Products,[37] which we designate as resist materials r61, r63, r71, and r81. These are optically clear UV curable pre-polymer materials with relatively low viscosities and good adhesion to glass, metal, and polymer surfaces (depending on the formulation) with a relatively long shelf life. The materials have viscosities ranging from 0.2 to 2.5 Pa·s (or 200 to 2500 cP) and exhibit a high sensitivity to long-wavelength UV radiation (UVA, 365 nm). Once cured, the resulting solid networks have a rather high modulus, ranging from 0.4 to 1.6 GPa for a typical cure, and become remarkably insoluble to an array of solvents (including toluene, methanol, hexane, and methyl ethyl ketone but excluding chlorinated solvents). However, the uncured resins are soluble in ethanol and acetone, which we use as developers (acetone should be used sparingly as it swells the precured material moderately). For convenience, we utilize readily available commercial resists rather than custom designed thiolene formulations.

The experimental setup used is depicted in Figure 1. It consists of a long wavelength UVA source, a photomask, and the prepolymer resin sandwiched between two surfaces separated by a gasket. The UV source is a 365-nm Spectroline SB-100P flood lamp, equipped with a 100-W mercury lamp (Spectronics, NY). When higher collimation is necessary (imaging of small feature sizes), we employ an Oriel flood illumination system (no. 87532-1000, Oriel Instruments, CT) equipped with a 500-W Hg(Xe) lamp, providing a 2.6° collimation angle and a ±5% beam uniformity. Deep or near UV configurations are available by a selection of suitable dichroic mirrors (for 350 to 450 nm, we use nos. 80112 and 80512, Oriel Instruments, CT) or filters. Photomasks are designed with a computer graphics program and are printed on transparencies (CG3300, 3M) using a black and white 1200-dpi laser printer (Laserjet 8000N, Hewlett-Packard). To fabricate tall structures (over 1 mm), several transparencies (2−4) are aligned in registry and stacked, resulting in a higher optical density photomask.[38]

The resist was placed either between two glass plates or between a glass plate (top surface) and cured PDMS (bottom surface) with a spacer between them. We used $75 \times 50 \times 1$ mm^3 glass plates (Corning Microslides, plain, model no. 2947). For samples with a thickness under 1 mm, silicon wafer slivers (400- or 600-μm thick, from Wafer World, FL) were used as spacers; for thicker samples, cured PDMS membranes of well-defined thickness were cut in frames and used as gasket materials. Photocuring was carried out in a fume hood, for different exposure times t and sample-to-lamp distances L (detailed in the following). The photocuring process consists of a UV pre-cure through a mask (which defines the patterned lateral and vertical dimensions), a rinse with acetone and ethanol (which removes un-cross-linked material), and a final UV post-cure (without a mask, with a dose 20 to 30 times that of the pre-cure) and thermal cure, which further cross-links the material and enhances its adhesion to the substrate. The patterned height can be defined by the spacer height[12] or varied continuously by the administered UV dose, as described in the following.

The transmissions of the relevant materials to 365-nm UV were first measured with a digital radiometer Spectroline DRC-100X equipped with a DIX-365A UV-A sensor (both Spectronics, NY). This sensor covers the spectral range 320−400 nm, relevant to this photopolymerization, with an intensity range of 0−20 000 μW/cm^2 and 10 μW/cm^2 resolution.[39] The transmission of a sheet of material of thickness x and attenuation coefficient μ is given by the ratio of the transmitted and incident intensities, namely, the Beer−Lambert law, $T(x) \equiv I(x)/I(0) = \exp(-\mu x)$. With a series of 10 experiments (corresponding to different specimen thicknesses) for each material, we obtained μ(glass) = 0.066 mm^{-1}, μ(transparency) = 2.08 mm^{-1}, and μ(uncured resists) ≈ 0.13−3.1 mm^{-1}, depending of the formulation. This corresponds to transmissions of $T = 0.94$ and $T = 0.80$ for a single glass slide (thickness $x = 1.0$ mm) and a single transparency ($x = 105$ μm), respectively. The exposure dose (product of time and intensity, dose = tI in units of J/cm^2) received by a specimen is given by the product of the incident dose with the transmissions of the middle windows. Typically, dose = $tI(0)\,T(glass)\,T(transparency)^2$, for one glass slide and two transparencies aligned in register. The flood lamp is mounted on a vertical rack such that the sample-to-lamp distance L varies from $L \approx 6-60$ cm, corresponding to a sample surface intensity of, respectively, 12.5 mW/cm^2 to 250 μW/cm^2. The enhanced collimation and illumination uniformity at large distances comes at the expense of an intensity decay ($\approx 1/L^{1.6}$) of this flood lamp.

Depth of Cure. A series of experiments were carried out to determine the dependence of the patterned feature height on the administered UV dose. A photomask consisting of an array of 10 lines, 2-mm wide and 25-mm long, was printed, as described previously. A deep layer (several millimeters) of resist material was confined inside a PDMS gasket and covered with a glass slide and photomask. Each line was UV-exposed for increasing amounts of time using a sliding shutter at a fixed sample-to-lamp distance. The top glass plate (where the cross-linked material is patterned) was then slowly removed from the nonadhering PDMS workspace, leaving the majority of the un-

(32) Jacobine, A. F. In *Radiation Curing in Polymer Science and Technology*; Fouassier, J.-P., Rabek, J. F., Eds.; Elsevier Applied Science: London, 1993; Vol. 3, Chapter 7.

(33) (a) Cramer, N. B.; Scott, J. P.; Bowman, C. N. *Macromolecules* **2002**, *35*, 5361. (b) Cramer, N. B.; Davies, T.; O'Brien, A. K.; Bowman, C. N. *Macromolecules* **2003**, *36*, 4631. (c) Cramer, N. B.; Reddy, S. K.; O'Brien, A. K.; Bowman, C. N. *Macromolecules* **2003**, *36*, 7964.

(34) Wilderbeek, H. T. A.; Goossenst, J. G. P.; Bastiaansen, C. W. M.; Broer, D. J. *Macromolecules* **2002**, *35*, 8962. Wilderbeek, H. T. A.; Teunissen, J. P.; Bastiaansen, C. W. M.; Broer, D. J. *Adv. Mater.* **2003**, *15*, 985.

(35) Pojman, J. A.; Varisli, B.; Perryman, A.; Edwards, C.; Hoyle, C. *Macromolecules* **2004**, *37*, 691.

(36) Certain commercial equipment, instruments, or materials are identified in this paper to specify the experimental procedure adequately. Such identification is not intended to imply recommendation or endorsement by the National Institute of Standards and Technology, nor is it intended to imply that the materials or equipment identified are necessarily the best available for the purpose.

(37) *Technical data sheet for NOA optical adhesives*; Norland Products, Inc.: New Brunswick, NJ.

(38) Higher mask resolution or optical density maybe required to fabricate respectively smaller feature sizes (down to 25-μm line width) or taller structures (up to several millimeters). In that case, we outsource the photomask to an image-setting graphic company. Photomasks produced by a Herkules imagesetter (Heidelberg, Germany) offer a 5080 dpi resolution and optical density of 4.25.

(39) "Light intensity" is used here instead of "energy fluence rate" or "irradiance", in units of W/m^2. It is related to the "photon fluence rate" [einstein m^{-2} s^{-1}] by $E = N_A hc/\lambda$, where E is the energy per mole of photons [J mol^{-1}], N_A is the Avogadro number, h is Planck's constant, c is the speed of light, and λ is the radiation wavelength.

cross-linked material on this bottom surface. The un-cross-linked material on the glass plate was rinsed with an ethanol/acetone mixture (1:1 volume ratio) by gently blowing compressed air and rinsing with ethanol. The pre-cured pattern was then UV post-cured using at least 20 times the pre-cure dose. To expedite the process (and because post-cure does not require collimation), short (10 cm) sample-to-lamp distances L were used, resulting in higher intensity and short exposure times. At distances shorter than 10 cm, the heat generated by the mercury lamp can induce delamination before full cross-linking. The height of the patterned structures below 1 mm was measured with a Dektak 8 profilometer (Veeco, CA) using a 2.5-μm stylus and, otherwise, with a digital caliper (Digit-cal MK IV, Brown & Sharpe, RI).

This procedure was carried out for resists r61, r63, r71, and r81, for L ranging from 10 to 61 cm and t ranging from 10 to 2700 s, covering a wide UV dose window from 10^{-3} to 2.5 J/cm^2. This series of experiments yields a relationship between the patterned height h and the administered UV dose (after correcting for the absorption of the mask and top glass plate). The standard dose uncertainty, as a result of lamp intensity oscillation and radiometer reading, is typically less than 5%.

Transmission During Photocuring. A second series of experiments monitored the transmission of resist layers of constant thickness during photocuring. Multiple samples (3−14, for each resist) of various thicknesses and ranging from 20 μm to over 3 mm were cast between glass plates and confined within PDMS or silicon gaskets. A radiometer was placed immediately below the specimen during thorough UV exposure, and the dose was recorded in situ (correcting for the top glass window and mask, but subtracting the bottom plate). A possible UV rate effect was ruled out by monitoring the transmission of identical specimens subject to different incident intensities (by varying the lamp-to-sample distances from 10 to 61 cm) and recording exposure time (yielding dose) and transmitted intensity independently. The superposition of transmission data indicated that the UV dose is the relevant timelike parameter. Exposure doses (corrected for attenuation) ranged from 0.6 mJ/cm^2 to 77 J/cm^2 and were obtained from a combination of exposure time ($1 \le t \le 12\,000$ s) and incident intensity ($645 \le I_0 \le 9600$ μW/cm^2) intervals.

Microfluidic Device Fabrication. Photomasks were designed and printed on transparency slides as described above. A 600-μm-thick layer of resist r81 was then patterned between a glass plate and a cured PDMS substrate and confined within a PDMS gasket. To produce a two-level channel structure, two masks and two illumination steps were employed in sequence. A first mask was placed over the glass plate, and the sample was exposed to 9.0 ± 0.5 mJ/cm^2 (using incident $I_0 = 220$ μW/cm^2). The second mask was placed on top, and curing proceeded for an additional 15.1 mJ/cm^2. The patterned resist material on glass was slowly separated from the bottom surface, and the un-cross-linked material was washed away using a 1:1 (volume ratio) ethanol/acetone mixture and by carefully blowing compressed air. The patterned resist on glass was post-cured using an additional 1.0 J/cm^2 (under 5 min at $I_0 \approx 5$ mW/cm^2, $L \approx 10$ cm) and thermally cured for 12 h at 50 °C to increase its durability. Note that the overall process (excluding the optional thermal cure) takes about 15 min. The resulting *master* was placed inside an aluminum foil tray for PDMS replication. Approximately 8 mL of Sylgard 184 (Dow Corning, MI) pre-polymer with a 10:1 mass ratio of base to curing agent was mixed thoroughly, degassed under vacuum, poured over the master, and cured in a convection oven at 75 °C for 1 h. The PDMS replica was cut with a scalpel and peeled off the master, and holes were bored with a flat needle for inputs and outputs. To irreversibly seal the device against glass, a glass plate and the PDMS patterned surface were UV−ozone cleaned using a 342 UVO (Jelight, CA). The glass plate was exposed for 30 min, and the PDMS slab was exposed for the last 90 s, before bringing the two clean surfaces into contact and curing the device for an additional 4 h in a convection oven at 75 °C. Stainless steel connectors were introduced in the bored holes and coupled to computer-controlled syringe pumps via Tygon tubing.

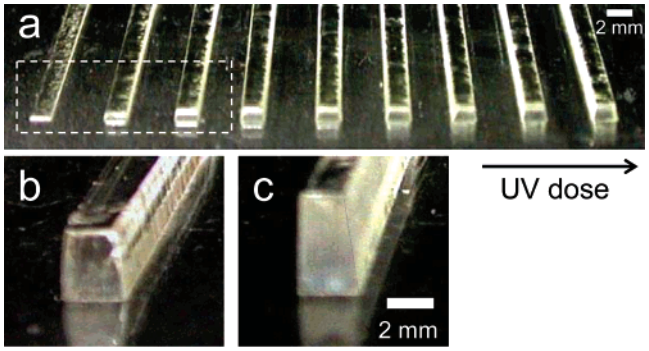

Figure 2. Patterned lines on a glass substrate evidencing the frontal nature of the photopolymerization: dependence of feature height h on the UV dose. (a) Resist lines (r81) exposed for discrete UV doses within a 50−640 mJ/cm^2 window (increasing from left to right); dashed rectangle emphasizes the fast onset of growth. Detail of resist (b) r71 and (c) r63 lines upon 300 and 280 mJ/cm^2 UV exposure, respectively. The resist spacer was taller than any of the patterns.

Results and Discussion

Frontal Kinetics. The first series of experiments establishes the frontal nature of the photopolymerization process. Figure 2 shows micrographs of arrays of patterned lines on the same glass plate exposed for different times, t. A well-defined interface between the polymerized solid and the liquid pre-polymer, characteristic of frontal polymerization, becomes evident after development (selective washing) takes place. The feature height was found to depend solely on the UV exposure because the spacer used (cf. Figure 1) was considerably thicker (10 mm) than any of the patterned lines.

The impact of development on the patterned features, in terms of washing "duration" (exposure time to solvents) and "solvent quality" (ratio of ethanol and acetone), was carefully investigated. Our results indicated that the resulting height h is largely insensitive to the development procedure, implying a sharp solid−liquid boundary. This front stems from the high optical attenuation and restricted (mass and heat) transfer processes in the photopolymerization. Its sharpness is likely to be favored by the step-growth polymerization kinetics, in which molecular weight M_r increases suddenly at high monomer conversion.

Despite the relevance of FPP, quantitative measurements of the propagation of photopolymerization fronts are surprisingly scarce, as recognized previously.[27] The definition of frontal position, in particular, is often unclear. Our method of locating the "cure depth" or "front position" $h(t)$ is quite straightforward: it corresponds to the thickness of the solidified material after exposure of the sample to light and subsequent development. This criterion[18,40] is evidently suitable for characterizing and controlling feature depth in RP applications. Other methods include depth-resolved hardness and[40,41] interferometric[31] or spectroscopic measurements.[13] In the former method, depth of cure is defined by extrapolating to a point of zero hardness, and good agreement is obtained with a procedure similar to ours.[40] We next introduce a minimal FPP model that is used to interpret our experimental results.

FPP Model. Photopolymerization commences with the absorption of light, which generates the necessary reactive

(40) Cook, W. D. *J. Macromol. Sci., Chem.* **1982**, *A17*, 99; *J. Appl. Polym. Sci.* **1991**, *42*, 2209.
(41) Hirose, T.; Wakasa, K.; Yamaki, M. *J. Mater. Sci.* **1990**, *25*, 1209.

species for chain initiation. Usually, the process requires the addition of (strong light-absorbing) photoinitiators to the monomer that are consumed during polymerization. The light intensity decays from the illuminating surface, which translates into a decaying initiation rate profile. In the commonly discussed "photobleaching" photopolymerization, the photoinitiator is consumed near the surface (and if the high optical absorption and limited mass transfer conditions are also met), the light absorption decreases, and the polymerization front proceeds toward the bulk, resulting in FPP. These observations have led to an emphasis on the modeling of photoinitiation in stable planar FPP. However, it has been recognized that frontal polymerization may occur without photobleaching,[28] as long as the matrix (constituted by monomer and polymer) is absorbing. Actually, some FPPs are initiator-free,[10] and this is indeed achievable in thiolene systems.[33a] In our own measurements, we observe an increase in the optical attenuation upon light exposure so that the photobleaching model is clearly not applicable to our system. We, thus, develop a model that accounts also for this "photodarkening" effect.

As discussed above, a number of photopolymerization models have recently addressed the chemistry and reaction kinetics of FPP.[13,16−18,27−31,42] Comprehensive treatments include at least four reaction steps: photolysis, chain initiation, propagation, and termination. For practical reasons, these usually exclude mixing due to flow (convection) or diffusion, temperature, or any kinetic complications, such as diffusion-limited propagation and termination, or auto-acceleration or deceleration processes that may accompany frontal propagation. When multifunctional monomers are used, network formation (gelation) and the associated slowing of kinetics becomes an important factor.[10] On the other hand, experimental studies typically focus on the effect of a *single* variable, such as the light intensity, monomer functionality and reactivity, and photoinitiator concentration. Given the complexity of realistic FPP processes, we have opted to develop a "minimal" model aiming at understanding and controlling frontal kinetics for our lithographic RP applications. Our model has obvious mathematical commonalities with classical treatments of photopolymerization[43,44] but focuses directly on observable properties relevant to device fabrication: the front position $h(t)$, as defined by the solid/liquid interface, the light transmission of the resist layer, and the optical attenuation constants of the monomer and the fully converted material.

First, we introduce a dynamic order parameter variable $\phi(x, t)$, describing the spatio-temporal variation of the monomer converted to polymer (i.e., conversion fraction) and the light transmission $T(x, t)$ of the resist layer; x is the depth from the illuminated surface (defined $x \equiv 0$), and t [s] is exposure time (proportional to the UV dose = $I_0 t$). This dimensionless *extent of polymerization* $\phi(x, t)$ describes the ratio of photopolymerized versus unpolymerized units, at a certain depth x and time t; it lies in the interval $0 \leq \phi \leq 1$ and has limiting behavior $\phi(x, t \rightarrow 0) = 0$ and $\phi(x, t \rightarrow \infty) = 1$ (i.e., full conversion) for all $x > 0$. The rate of change of $\phi(x, t)$ with t is proportional to the light intensity $I(x, t)$ [J cm^{-2}], the amount of material available for conversion $1 - \phi(x, t)$, and the reaction conversion rate K [cm^2 (J s)$^{-1}$],

$$\frac{\partial \phi(x, t)}{\partial t} = K[1 - \phi(x, t)]I(x, t) \tag{1}$$

The assumption that K is constant (i.e., independent of t or x) throughout the process holds in the absence of reaction "feedback", which may give rise to acceleration or deceleration, as mentioned above. Once photopolymerization has commenced, the material becomes a two-component system (consisting of reacted and unreacted material), which do not generally have the same optical attenuation coefficient μ [mm^{-1}]. We, therefore, model the light intensity (or transmission) profile with depth as a two-component Beer−Lambert law,

$$\frac{\partial I(x, t)}{\partial x} = -\bar{\mu}(x, t)\, I(x, t) \tag{2}$$

with an effective attenuation coefficient

$$\bar{\mu}(x, t) \equiv \mu_0[1 - \phi(x, t)] + \mu_\infty \phi(x, t) \tag{3}$$

defined as the arithmetic average of the attenuation coefficients of the unexposed monomer (μ_0) and fully polymerized (μ_∞) material. Equation 2 evidently involves a mean field approximation valid when the "components" are randomly mixed. The usual Beer−Lambert law $\partial I(x)/\partial x = -\bar{\mu} I(x)$ or $I(x) = I(0)\exp(-\bar{\mu}x)$ is recovered for short and long times as $\bar{\mu}(x, t \rightarrow 0) = \mu_0$ and $\bar{\mu}(x, t \rightarrow \infty) = \mu_\infty$ for all $x > 0$. As photocuring proceeds, the conversion fraction $\phi(x, t)$ increases with time until it reaches a certain "critical conversion" ϕ_C ($\ll 1$), at which the (partially) converted material becomes a solid:

$$\begin{cases} \phi(x, t) > \phi_C, & \text{solid} \\ \phi(x, t) < \phi_C, & \text{liquid} \end{cases} \tag{4}$$

This threshold involves a combination of solidification through polymerization (specifically network formation or cross-linking, for multifunctional monomers) and glass formation processes.

Equations 1 and 2 define a system of nonlinear partial differential equations whose solution depends on four material parameters: the attenuation coefficients, μ_0 and μ_∞; the conversion rate KI_0; and the critical conversion ϕ_c. The former two parameters can be measured independently with a series of transmission measurements of uncross-linked and fully cross-linked specimens of different thicknesses. K is determined by the polymerization chemistry and ϕ_c is a structural variable, yet both can be obtained as fitting parameters. The former has been the focus of much of the previous research[7−10,27−33] and is, therefore, not emphasized in the present paper. For convenience, we use dimensionless intensity, that is, transmission $T(x, t) \equiv I(x, t)/I_0$ of a layer of thickness x at time t, to represent our results. We consider three cases, depending on the relative magnitude of the final and initial attenuation coefficients: (I) "photoinvariant" polymerization ($\mu_0 = \mu_\infty \equiv \bar{\mu}$), (II) "photobleaching" ($\mu_0 > \mu_\infty$), and (III) "photodarkening" ($\mu_0 < \mu_\infty$). The simplest case of constant attenuation with time (I) can be solved analytically and provides great insight into the process. The conversion fraction in this case equals

$$\phi(x, t) = 1 - \exp[-KI_0 \exp(-\bar{\mu}x)t] \tag{5}$$

The position of the moving *front* (solid/liquid interface) is defined through the condition

$$h(t) \equiv x(\phi = \phi_C) \tag{6}$$

(42) Lyubimova, T.; Righetti, P. G. *Electrophoresis* **1993**, *14*, 191.
(43) Wegscheider, R. *Z. Phys. Chem. CIII* **1923**, *103*, 273.
(44) Mauser, H. *Z. Naturforsch. B* **1967**, *22*, 569.

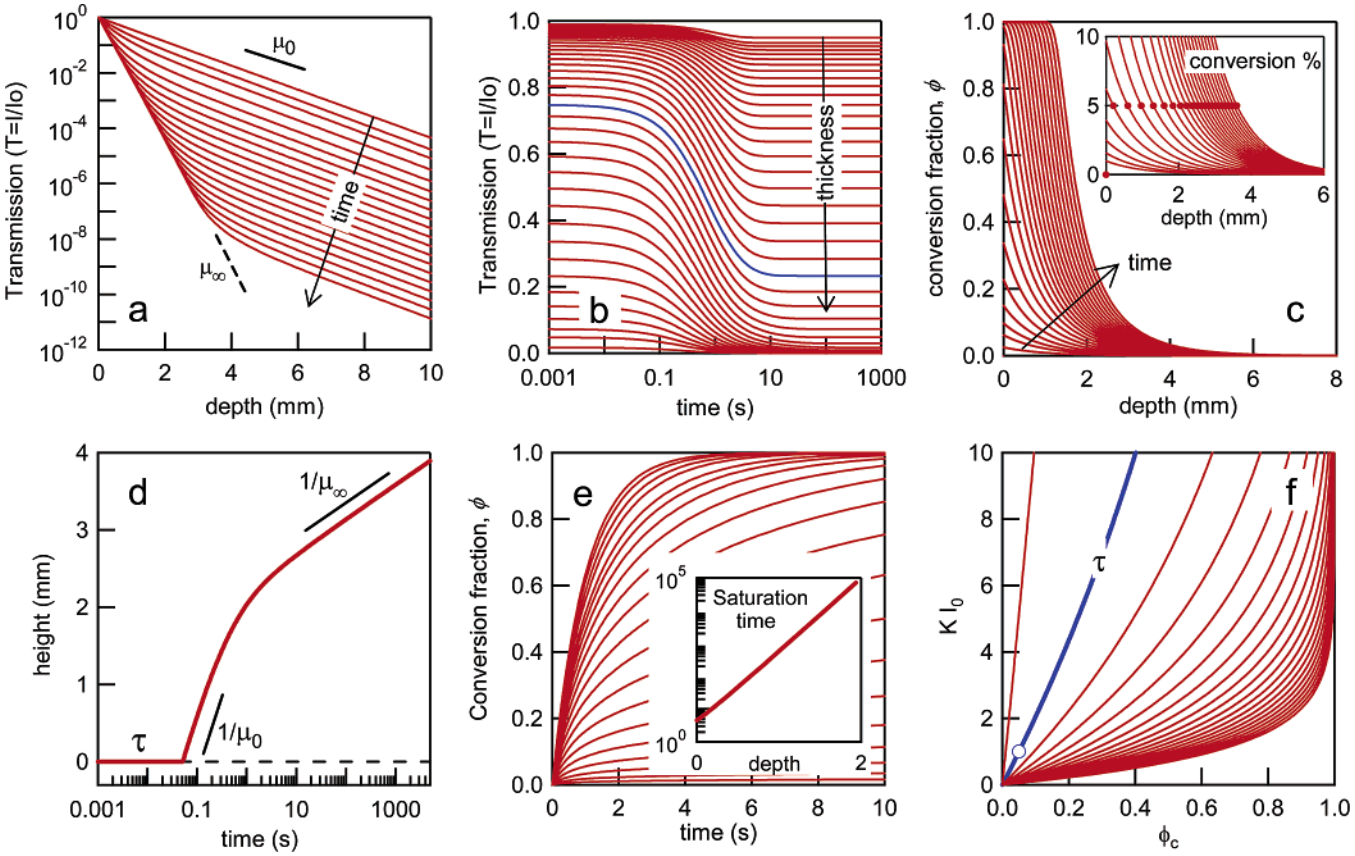

Figure 3. FPP spatio-temporal modeling of "photodarkening" with parameters $\mu_0 = 1\ \mathrm{mm}^{-1}$, $\mu_\infty = 5\ \mathrm{mm}^{-1}$, $KI_0 = 1\ \mathrm{s}^{-1}$, and $\phi_c = 5\%$. (a) Transmission $T(x, t)$ dependence on depth x during photocuring (time, t); a simple Beer−Lambert law is recovered in the short and long time limits, with attenuation coefficients μ_0 and μ_∞, respectively. (b) $T(x, t)$ dependence on t plotted for selected sample thicknesses x; the long-time plateau corresponds to full conversion. (c) Extent of conversion $\phi(x, t)$ dependence on depth x and time t. The inset details the intersection of the solid conversion threshold ϕ_c with $\phi(x, t)$, defining the front position $h(t)$ and, thus, the patterned vertical dimension. (d) Frontal kinetics: feature height $h(t)$ dependence on t, exhibiting logarithmic growth at short and long times, with proportionality constant $1/\mu$ and a broad intermediate crossover. An induction time τ precedes the onset of frontal propagation. (e) Conversion order parameter $\phi(x, t)$ dependence on t, calculated for various x. Inset: saturation time τ_{sat} defined by a 99% (or "full") conversion condition grows exponentially with depth x. (f) Induction time τ as a function of conversion rate KI_0 and ϕ_C. Marker indicates τ found from (KI_0, ϕ_c) above, and the lines correspond to constant τ ranging from 0.01 to 1 s.

so that $\phi_C = 1 - \exp[-KI_0 \exp(-\bar{\mu}h)t]$. Thus, the patterned height $h(t)$ grows *logarithmically* with time,

$$h(t, \bar{\mu}, KI_0, \phi_C) = \frac{\ln(t/\tau)}{\bar{\mu}} \tag{7}$$

where

$$\tau(KI_0, \phi_C) \equiv \frac{\ln[1/(1 - \phi_C)]}{KI_0} \tag{8}$$

The formation of a solidification front does not occur instantaneously with light exposure, and a time τ for ϕ to first approach ϕ_C is required before the front starts propagating from the illuminated surface so that eq 7 applies for $t > \tau$. The *induction time* τ is, thus, the t required for the surface layer ($x = 0$) to first become a solid, that is, $\phi\ (x = 0, \tau) = \phi_C$.

Despite the apparent simplicity of eqs 1 and 2, these coupled *nonlinear* equations cannot be solved exactly in closed analytic form except for special limits, such as the simple case just described where $\mu_0 = \mu_\infty \equiv \bar{\mu}$. However, the physically important case where μ evolves in time (photobleaching and photodarkening) can be solved numerically. Figure 3 illustrates the solution obtained for a photodarkening process using the realistic model parameters $\mu_0 = 1\ \mathrm{mm}^{-1}$, $\mu_\infty = 5\ \mathrm{mm}^{-1}$, $KI_0 = 1\ \mathrm{s}^{-1}$, and $\phi_C = 0.05$ (or 5%). These results are obtained by the discretization of eqs 1 and 2, followed by the incremental propagation of their solution in time using IGOR Pro 4 (WaveMetrics, OR); depth and time intervals of $10^{-3} < x < 15$ mm and $10^{-3} < t < 10^7$ s were sampled in logarithmic increments. The resist transmission $T(x, t)$ as a function of depth (or thickness) for various curing times is computed in Figure 3a. In the short and long time limits, the usual Beer−Lambert law holds and the intensity decays exponentially in x with attenuation coefficients μ_0 and μ_∞, respectively. At intermediate times, there is a crossover between these two asymptotic regimes. (An attempt to fit experimental transmission results with the simple Beer−Lambert law would result in an unphysical ($\neq$1) intercept for infinitely thin films, symptomatic of the necessity of accounting for the variation in μ in the course of photopolymerization.) Figure 3b depicts the transmission decrease and eventual asymptotic saturation during photocuring, as a function of specimen thickness. The spatio-temporal variation of the conversion fraction is shown in Figure 3c. The front position $h(t) \equiv x(\phi = \phi_C)$ at 5% conversion is indicated by the solid markers. It defines the depth at which the conversion profile first exceeds ϕ_C. The resulting time-dependent front position, generated by the (h, t) pairs, is shown in Figure 3d. As anticipated from eq 7, the front moves logarithmically at "short" and "long" times where $\bar{\mu}(x, t \to 0) \approx \mu_0$ and $\bar{\mu}(x, t \to \infty) \approx \mu_\infty$, respectively. In the

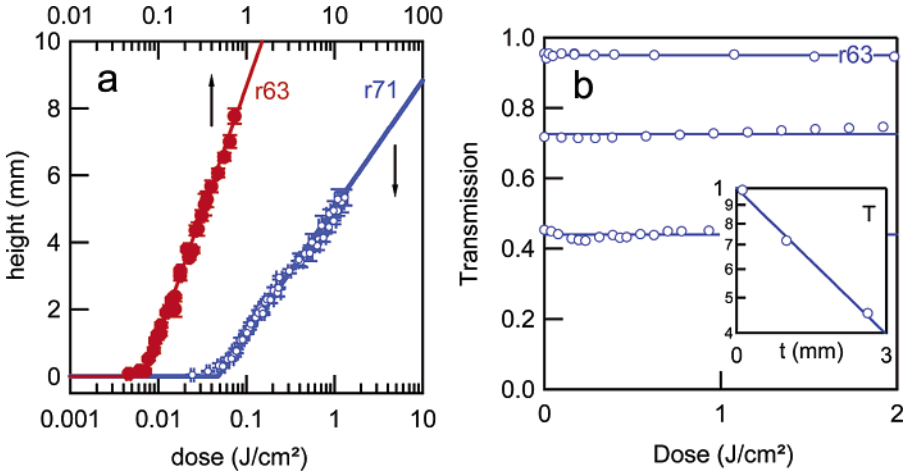

Figure 4. "Photoinvariant" polymerization: frontal kinetics of resist materials whose transmission remains constant upon UV exposure. (a) Experimental data of pattern height as a function of UV dose, h(dose), for resists r63 (●) and r71 (○). The solid lines are model fits according to eq 7. (b) Light transmission (shown for r63) measured for three resist thicknesses (120 μm, 1.00 mm, and 2.63 mm) during photocuring. Inset: Beer−Lambert representation and calculation of attenuation coefficient μ. This (independently measured) parameter is introduced in the h(dose) fit shown in part a.

present photodarkening case (i.e., $\mu_0 < \mu_\infty$), the front moves faster initially ($\propto 1/\mu_0$) and slows down ($\propto 1/\mu_\infty$) at later times. Thus, the frontal propagation is logarithmic in time, as in eq 7, but there is a transition in the slope as μ evolves from its monomer value at short times to its polymerized value at long times. The situation is reversed for partial photobleaching, where the front accelerates at later times. For *total* photobleaching, where the polymerized material is fully transparent to radiation ($\mu_\infty = 0$), the frontal movement changes from logarithmic in time at short times to *linear* in time at long times (rather than logarithmic) so that the velocity is asymptotically constant. This is another limit (fixed-point solution) in which eqs 1 and 2 can be solved exactly.

We emphasize here that these fronts *do not* involve autocatalytic reactions that sustain their frontal movement.[15,35] Such fronts happen to propagate with a constant velocity under normal circumstances, but these fronts have a completely different physical origin. A general property that both autocatalytic and FPP fronts are likely to share is a tendency of the stable planar fronts to become *unstable*[45] at high propagation rates or other conditions leading to interfacial instability (e.g., large mismatch in density or viscosity of materials on each side of the front, gradients in surface tension due to thermal gradients or composition gradients, static heterogeneities, etc.).

In addition to the induction time τ, it is natural to define a "saturation time" τ_{sat} as the time required for full conversion of the resist layer of a given thickness. For this purpose, we plot (Figure 3e) the t dependence of the conversion fraction for various depths and compute a 99% conversion condition (inset), which we find to vary exponentially with depth. We finally consider the "induction time" τ and verify that it is rather well approximated by eq 7 even for our photodarkening system because $\bar{\mu}(x, t \to 0) \approx \mu_0$. Its magnitude is determined by KI_0 and ϕ_c. For $KI_0 = 1\ s^{-1}$ and $\phi_C = 5\%$, we obtain an induction time of 50 ms, indicated by an open marker. The solid dark line corresponds to (KI_0, ϕ_C) pairs that share the same induction time, while the other lines span a τ range from 0.01 to 1 s. The specific (KI_0, ϕ_C) values are determined by combining transmission $T(x, t)$ and height $h(t)$ data, shown in Figure 3b,d.

Next, we report on experimental findings using four thiolene-based resists and utilize the proposed model to interpret and quantify them. For clarity, we use UV dose (the product of exposure time and light intensity, dose ≡ $I_0 t$) instead of t in the following discussion. Equation 1 can, thus, be written

$$\frac{\partial \phi(x, \text{dose})}{\partial \text{dose}} = K[1 - \phi(x, \text{dose})]T(x, \text{dose}) \qquad (9)$$

and the results (5−8) remain identical, apart from the replacement, t = dose/I_0. As a control measurement, we have carried out cure depth h experiments with various fixed incident light intensities I_0 and exposure time intervals t and found that all the data superimposed using the time−dose relation just given. Thus, the conversion rate does not appear to depend on I_0, as has been reported in other UV curable systems.[10,41]

Transmission and Front Position During Photocuring. During photocuring, the initial homogeneous resist undergoes a complex spatio-temporal change, emanating from the illuminated surface and resulting in a depth- and time-dependent local transmission. We have measured *integrated* transmissions of specimens of constant thickness as a function of dose. The dose window investigated encompasses (and largely exceeds) the relevant UV range required for RP. In this range, for the four photo-cross-linkable resists studied, we have observed two cases: (i) photoinvariant polymerization, in which the transmission $T(x = \text{const}, t)$ remains constant and (ii) photodarkening, in which the $T(x = \text{const}, t)$ *decreases* during the reaction. No color change occurs in either case, our classification concerning only the variation of the optical transmission to the actinic (365 nm, in this case) radiation. Eventually, partial photobleaching was observed, at even higher UV doses (10−100 times larger than those of interest to our RP process). We are unaware of previous experimental or theoretical reports of this photodarkening phenomenon that is a conspicuous feature of our measurements. Photodarkening of these resists is caused by fluorescence emission in the visible range, which is concurrent to photoinitiation and eventually disappears upon exposure.[46]

Figure 4a presents height versus dose results obtained for the photoinvariant case, exhibited by resists r63 and r71, evident from the constant transmission (for selected

(45) Cross, M. C.; Hohenberg, P. C. *Rev. Mod. Phys.* **1993**, *65*, 851.
(46) Norland, E. Personal communication.

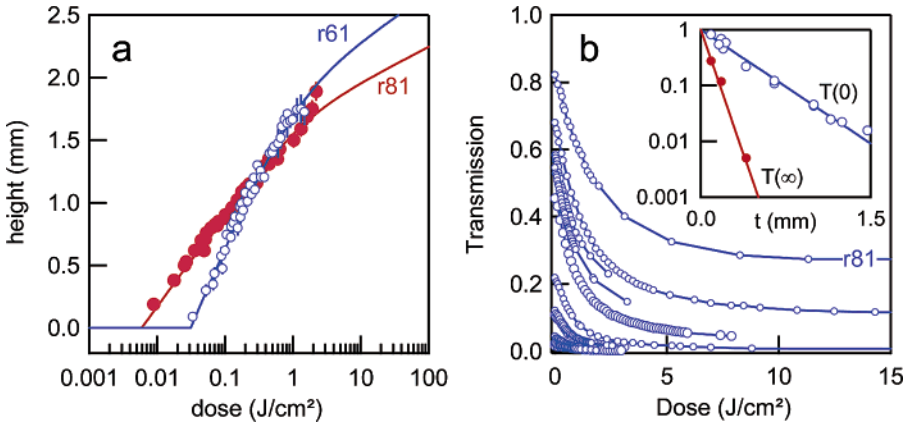

Figure 5. "Photodarkening" polymerization: resist transmission decreases during photocuring. (a) Front position h(dose) as a function of UV dose measured for resists r61 (○) and r81 (●) and model fit according to eqs 1, 2, and 6. (b) transmission $T(x = \text{const}, \text{dose})$ dependence on UV dose for specimens of various thicknesses (comprised between 60 μm and 1.475 mm). The inset is a Beer−Lambert plot of the sample transmission of the unexposed (time ≈ 0) and "fully exposed" material. The simple Beer−Lambert law is obeyed in these limits and the asymptotic attenuation coefficients μ_0 and μ_∞ are calculated and inserted into the fit (solid line) to the h(dose) measurements shown in part a.

thicknesses) shown in Figure 4b. The inset shows the usual Beer−Lambert representation of thickness-dependent transmission (obtained for r63 at long exposure times), which defines the attenuation coefficient $\bar{\mu} \equiv \mu_0 \approx \mu_\infty$. As expected from eq 7, the frontal kinetics shown in Figure 4a is logarithmic. The data could be described using $K = 0.2$ cm^2/J and $\phi_C = 1.4\%$ (r63) or 0.95% (r71) and using the experimentally measured attenuation coefficients, $\bar{\mu} = 0.304$ mm^{-1} (r63) and 0.599 mm^{-1} (r71).

For the photodarkening materials (resists r61 and r81) both the initial μ_0 and terminal μ_∞ attenuation coefficients were determined (shown for r81 in the inset Figure 5b). The *terminal* state was defined as the asymptotic limit in which the transmission reached a constant value. Next, K was fixed by fitting the transmission decay with time. Note that K is the only free parameter because μ_0 and μ_∞ are determined from independent experiments (and ϕ_c is unrelated to the transmission, T). Finally, we estimated the conversion threshold ϕ_C by fitting the experimental height versus dose measurements, shown in Figure 5a, keeping the remaining model parameters (μ_0, μ_∞, and K) constant. This procedure yields the complete set of parameters: $K = 0.55$ cm^2/J and $\phi_C = 1.7\%$ and $(\mu_0, \mu_\infty) = (1.78, 6.0)$ mm^{-1} for resist r61 and $K = 0.55$ cm^2/J and $\phi_c = 0.32\%$ and $(\mu_0, \mu_\infty) = (3.08, 8.0)$ mm^{-1} for resist r81.

Figure 5b suggests the possibility of a master curve reduction of the transmission dependence with dose for photodarkening materials. For this purpose, we redefine the T by subtracting its asymptotic value and normalizing it to its initial value, according to $[T - T(\infty)]/[T(0) - T(\infty)]$. This procedure indeed collapses all initial ("zero" dose) data to unity and final ("infinite" time) data to 0. The UV dose is reduced by a shift factor D(shift), which is adjusted to superpose the experimental data. A satisfactory data reduction is obtained for shift factors D(shift) depending logarithmically on thickness, as shown in Figure 6 (for resist r81). However, an inspection of eq 2 of our model reveals that a transmission data superposition is *not* valid in the whole UV dose (or time) range. The reduction demonstrated in Figure 6 is, thus, strictly valid within a limited dose (lower part, in this case) window. Next, we demonstrate the value of understanding the frontal growth process by fabricating a model microfluidic device with a priori prescribed dimensions.

Multilevel Fluid Handling Device. We have recently reported on the RP of in-plane (two-dimensional) devices using photopolymerization and demonstrated two alter-

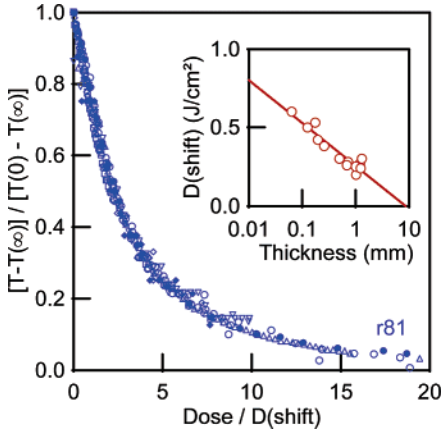

Figure 6. Master curve reduction (see text) of transmission measurements of a photodarkening resist (r81, data shown in Figure 5b). The UV dose shift factor dependence on thickness is depicted in the inset and is approximated to a logarithm. Despite the satisfactory data superposition in this UV dose window, such a reduction is not valid over the whole dose (time) range.

native methodologies, which we termed "open" and "close-faced".[12] The former fabricates masters patterned on glass, which are then replicated by PMDS molding and irreversibly sealed against a glass plate. The latter fabricates *devices*, consisting of a patterned polymer matrix confined between glass plates, involving just one step. This process is similar to the "ultra rapid prototyping" proposed by Beebe and co-workers.[47] However, the use of thiolene-based resists offers the additional advantage of negligible oxygen inhibition and wider organic solvent resistance, expanding the range of applications of this technology. We demonstrated patterning of structures taller than 1 mm and microchannels with line widths down to 50 μm.[12] In addition, we showed that resist confinement (which need not be spun-cast) could yield nonplanar structures with height gradients. In this paper, we seek to demonstrate the merits of FPP in the fabrication of more complex microfluidic structures.

The previous sections characterized and modeled in "minimal" terms the frontal kinetics necessary for an efficient application of FPP to RP. We select the open-faced methodology and one of the resist materials (r81),

(47) Khoury, C.; Mensing, G. A.; Beebe, D. J. *Lab Chip* **2002**, *2*, 50.

which exhibits faster cure at low UV doses. Upon UV exposure through an optical mask, stable planar polymerization fronts emanate from the top glass surface toward the bulk (Figure 1). To generate multilevel structures, light exposure should be modulated. This can be achieved through either binary (i.e., black and white) or gray-scale masks, although the latter requires a high printing resolution (small grain size). In line with the simplicity of our approach, we have opted to use two binary photomasks printed on a standard desktop printer. Two illumination steps are employed: the first using one mask and the second with the two masks juxtaposed. Alignment of the masks is trivial for the geometry chosen and density and size of the features. After selecting a target feature height, the light exposure dose is calculated from model parameters and data (Figure 5a), taking into account acetate mask attenuation (white). The printed mask (black) can be considered opaque (it has optical density of $\mathrm{OD} \equiv -\log(I/I_0) > 2$) for the patterned heights of interest here. The top glass plate is gently lifted with the cross-linked material (in fact, a *glass adhesive*) bonded to its surface. The pattern is carefully developed, removing liquid pre-polymer with minimal swelling of the illuminated portion of the (negative) resist layer.[11] The resulting *master* is depicted in Figure 7a. From stylus profilometry, we observe a bimodal structure having height features of 190 and 340 μm. Note that the resist layer (defined by spacers) was considerably taller, namely, 600 μm. A PDMS replica was produced, UV−ozone sealed against a flat glass plate, and then connected to fluid pumps, resulting in the microfluidic device shown in Figure 7b.

The device consists of a binary passive mixer, a T junction, and a series of flow constrictions. The mixer contains obliquely (45°) oriented grooves on the top wall of the channel, which induce mixing[20,21] by chaotic advection.[48] These passive mixers generate helical streamlines (the result of adding a transversal component to the longitudinal flow along the channel axis) in laminar flows, greatly accelerating mixing by stretching and folding co-continuous streams. The T junction involves two channels of different dimensions (lateral and vertical) but a nearly constant aspect ratio (1:1). Complex immiscible flows can be generated in simple T junctions[49] and flow focusing junctions[50] as a result of an interplay between interfacial tension and shear forces. The process is controlled by the relative flow rates and channel dimensions, which we were able to tune with FPP. Finally, the channel openings and constrictions generate extensional flow fields along the main channel. FPP, thus, provides a convenient route to the multilevel patterning required in complex microfluidic structures of controlled dimensions. The operation and measurements utilizing this and other devices will be reported in a separate publication.[51] Here, we briefly note that this device produces droplets of mixed components (A and B) of controlled size that are introduced into an immiscible flow (C). From the analysis of their deformation and relaxation, we obtain relevant fluid properties.

We have also explored the application of FPP to generate the needed organic solvent-resistant close-faced devices.[52] By controlling light exposure of both top and bottom surfaces, we fabricated microchannels with four identical walls having the same surface energy. In addition, self-supported polymer devices (with no glass or metal substrates) were fabricated using sacrificial PDMS release layers on both sides of the cross-linked polymer matrix. This fabrication process is notably not affected by the mechanical stresses and associated fracture or delamination that characterize supported fabrication methods. Our demonstration of the fabrication of dimensionally precise open- and close-faced devices illustrates the technological value and general applicability of controlled FPP for RP.

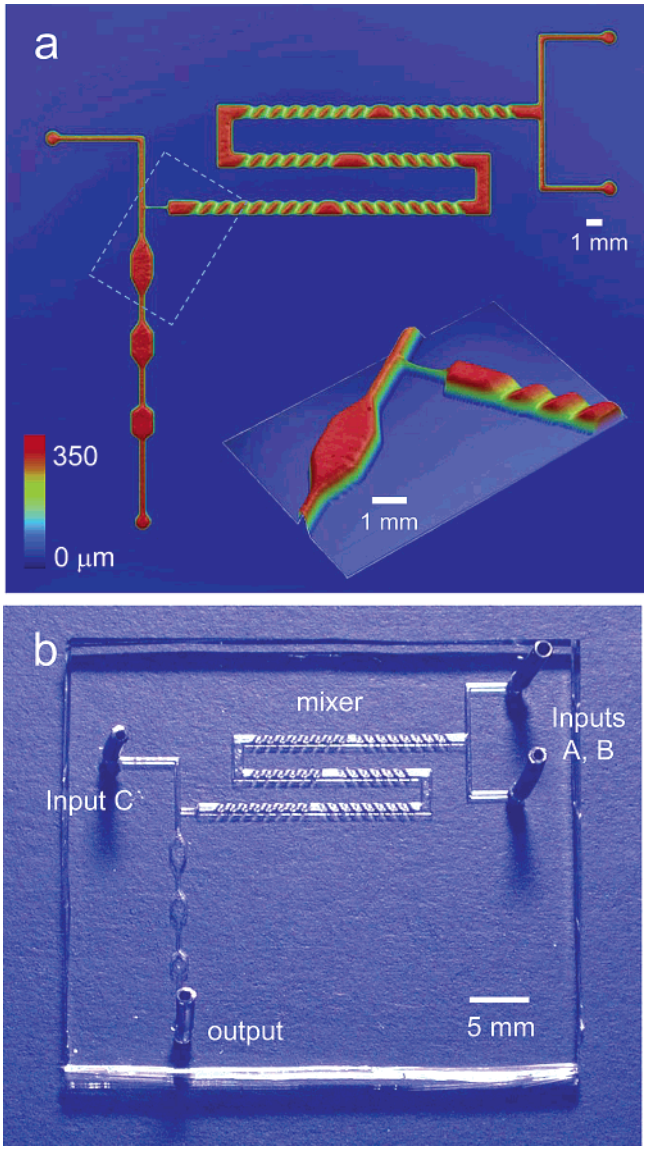

Figure 7. Microfluidic device fabricated by RP using FPP and a double photomask. (a) Profilometer scan of the multilevel device, incorporating a chaotic mixer, T junction, and a series of flow constrictions. Two heights were patterned: 190 μm (in mixer groves and one T junction arm) and 340 μm. (b) PDMS replica of the relief structure, irreversibly sealed against glass.

Conclusions

We recently developed a RP technique for the fabrication of microfluidic devices based on the contact lithography of a thiolene polymer resist.[12] The present work investigates the nature of the photopolymerization process underlying this promising fabrication methodology.

We find that the polymerization develops in a *wavelike* fashion from the illuminated surface of the resist material,

(48) Aref, H. *Nature* **1999** *401*, 756.
(49) Thorsen, T.; Roberts, R. W.; Arnold, F. H.; Quake, S. R. *Phys. Rev. Lett.* **2001**, *86*, 4163.
(50) Anna, S. L.; Bontoux, N.; Stone, H. A. *Appl. Phys. Lett.* **2003**, *82*, 364.
(51) Hudson, S. D.; Cabral, J. T.; Beers, K.; Amis, E. J. Manuscript in preparation.
(52) Wu, T.; Mei, Y.; Cabral, J. T.; Xu, C.; Beers, K. L. *J. Am. Chem. Soc.*, in press.

suggesting new approaches for exploiting this type of FPP process for microfabrication. The front position was determined by simply washing away the liquid form of the resist material exposed for a set UV dosage. We thoroughly measured the front position and its dependence on light exposure time and intensity and the variation of the optical transmission with time. These measurements indicate universal kinetics for the front displacement in time that motivated the formulation of our model. Surprisingly, the optical attenuation *increased* upon photocuring in some cases (photodarkening), while in others the attenuation remained essentially unchanged (photoinvariant polymerization). The former was caused by concurrent fluorescent emission, in addition to photoinitiation. Most experimental and theoretical studies have formerly addressed photobleaching polymerization, and we are unaware of any previous reports of photodarkening. We, thus, developed a minimal FPP model that directly addresses the kinetics of the growth front position and the change in optical attenuation in time under general circumstances. This spatio-temporal model involves an order parameter $\phi(x, t)$ describing the extent of conversion of monomer to polymer (solid) and the extent of UV attenuation, $T(x, t)$. Many aspects of the photopolymerization process derive from the changing character of the optical attenuation in the course of resist exposure to UV light. Development of the front occurs logarithmically in time after an induction period τ required to convert a critical extent of monomer ϕ_c to cross-linked polymer at the illumination boundary. We also predict a crossover in the logarithmic growth prefactor associated with the change in the optical attenuation "constant" $\mu(x, t)$ in the course of time, consistent with our measurements.

This coarse-grained model of FPP allows us to apply RP in new directions. To illustrate the potential of the method, we fabricate complex multilevel microfluidic devices with simplicity, rapidity (less than 15 min), and low cost. Both open-faced masters for replication and close-faced devices can be fabricated with only simple photomasks and controlled light exposure. The overall rate, qualitative kinetics of frontal propagation, and the ultimate optical properties of the polymerized material can be tuned by varying the composition of the resist formulation. While the resists chosen in the present study provide conveniently large cure depths, fast photocuring, and low oxygen inhibition, this methodology is applicable to essentially any FPP process.

Acknowledgment. We acknowledge Vladimir Entov (Russian Academy of Sciences) for early discussions on the modeling of FPP and John A. Pojman (University of Southern Mississippi) for pointing out useful references. We also thank Alamgir Karim and Eric J. Amis for helpful comments and continuous support throughout this project.

LA049501E